Theoretical Insights into Potential-Dependent C−C Bond Formation Mechanisms during CO_2 Electroreduction into C_2 Products on Cu(100) at Simulated Electrochemical Interfaces

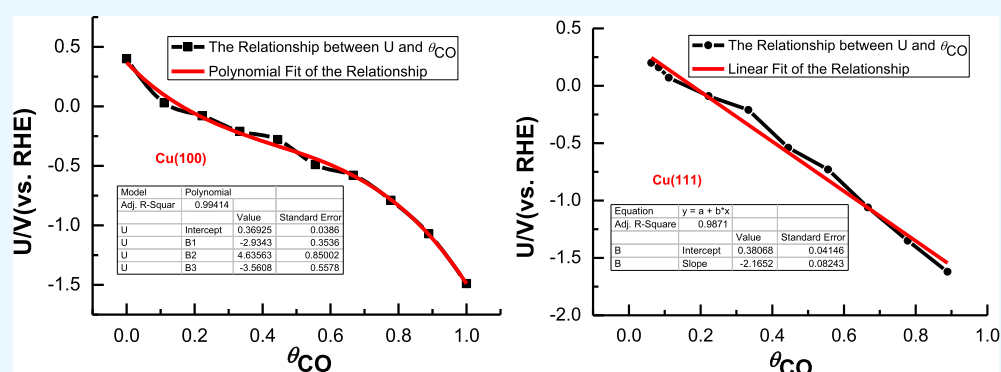Lihui Ou,* Zixi He, Hai Yang,* and Yuandao Chen

ACCESS | Metrics & More | Article Recommendations | SI Supporting Information

ABSTRACT: An improved CO coverage-dependent electrochemical interface model with an explicit solvent effect on Cu(100) is presented in this paper, by which theoretical insights into the potential-dependent C−C bond formation pathways occurring in CO_2 electrochemical reduction to C_2 products can be obtained. Our present studies indicate that CHO is a crucial intermediate toward C_1 products on Cu(111), and dimer OCCO is found to not be a viable species for the production of C_2 products on Cu(100). The reaction pathway of CHO with CO and CHO dimerization into dimers COCHO and CHOCHO may be C−C bond formation mechanisms at low overpotential. However, at medium overpotential, C−C bond coupling takes place preferentially through the reaction of COH with CO species and COH dimerization into dimers COCOH and COHCHO. The formed dimers COCHO, CHOCOH, and CHOCHO via reactions of CHO with CO, COH, and CHO species may lead to C_2 products, which are regarded as C−C bond formation mechanisms at high overpotential. The difference of obtained adsorption isotherms of CO on Cu(100) with that of Cu(111) may be able to explain the effect of the crystal face of Cu on product selectivity. The excellent consistencies between our present obtained conclusions and the available experimental reports and partial theoretical studies validate the reasonability of the present employed methodology, which can be also used to systematically study potential-dependent CO_2 electroreduction pathways toward C_2 products on Cu(100) or other metal catalysts.

INTRODUCTION

Electroreduction of CO_2 into hydrocarbons and alcohols on the Cu electrodes has been a remarkable topic of interest to both scientific and energy technology communities in recent years since it can be a promising candidate for a carbon-neutral and zero-emission energy cycle and thus mitigate the emission of CO_2 in the atmosphere,[1−5] in which the formation of C_2 products like C_2H_4 is particularly fascinating for energy conversion and storage in the chemical industry because of their higher energy densities than C_1 products, such as CH_4 and CH_3OH. Although CO_2 can be uniquely electrochemically reduced to hydrocarbons and alcohols on Cu electrodes, the required high overpotentials impede real application and spread of this technology.[6−10] Furthermore, the formation mechanism of C_2 products on the Cu electrodes needs more experimental and theoretical evidence and is still a subject of

ongoing discussion in recent decades. Understanding mechanisms of CO_2 electrochemical reduction to C_2 products can help design Cu-based alloy electrocatalysts that operated at relatively low overpotentials.

Cu(100) single-crystal surface had been experimentally reported to be especially selective toward C_2 products.[11] However, C−C bond formation mechanisms on this facet and the effect of electrode potentials on the mechanisms have been still indistinct at present.[12−16] Recently, many experimental

efforts have focused on C−C bond coupling mechanisms during CO_2 electroreduction on Cu(100) using *in situ* spectroscopic technologies, in which the adsorbed CO as a key reaction intermediate has been consistently identified.[17−20] Beginning with the adsorbed CO intermediate, different C−C bond formation mechanisms have been proposed. For example, a CO dimerization mechanism was proposed by Gattrell *et al.* as a C−C coupling pathway on Cu(100) on the basis of both infrared and surface-enhanced Roman spectroscopy.[21] Similarly, using online electrochemical mass spectrometry, the CO dimerization mechanism was also speculated on Cu(100) by Schouten *et al.*, in which C_2 species like C_2H_4 is preferably produced without simultaneous production of C_1 species, indicating that the electroreduction pathways of CO_2 into C_1 and C_2 products must bifurcate during initial CO reduction.[7,22] Using Fourier transformation infrared spectroscopy, a hydrogenated dimer intermediate OCCOH was detected by Pérez-Gallent *et al.* at the potential of *ca.* −0.10 V (*vs* RHE) during CO electroreduction on the Cu(100) electrode, followed by proton-coupled electron transfer.[19] The experimental studies on formation paths of the C−C coupled intermediate, however, have been limited in that the spectroscopically detected species must be relatively stable. Moreover, observable intermediates may be only spectators during CO_2 electroreduction.

Computationally, using various theoretical electrode/solution interface modeling, the facet dependence of products and C−C bond formation mechanisms on Cu electrodes were explored,[12,23−27] in which mechanistic understanding that is facile to be not obtained in experiments can be provided, and favored key intermediates can be identified toward the formation of C_2 products. For example, Asthagiri *et al.* reported facet dependence of CO_2 electrochemical reduction pathways on Cu electrodes using the linear kinetic barrier method based on Butler−Volmer theory with only one or two relaxed H_2O molecules.[23] Thereinto, COH formation is favored, by which CH_4 can be produced *via* CH_2 species at high overpotentials, whereas CHO formation on Cu(100) is preferred and C_2H_4 can be produced *via* C−C coupling of two CHO intermediates at relatively lower overpotentials. Calle-Vallejo *et al.* suggested that CO dimer on Cu(100) *via* an Eley−Rideal mechanism can be preferably formed on the basis of the computational hydrogen electrode model,[12] which is the relevant precursor to the production of C_2 species. However, this model to stabilize the CO dimer lacks the rigorous treatment of the electrode/solution interfaces. The computational studies from Nørskov *et al.* found that CO−CO coupling into the adsorbed OCCO intermediate is feasible on Cu(100) based on the like-capacitor model involving a single H_2O layer and cation,[24,25] which can be stabilized by the charged H_2O layer and play an important role during the production of C_2 below Cu potential of zero charge. Using constant electrode potential and computational hydrogen electrode models in the presence of implicit solvent, Head-Gordon *et al.* revealed that C−C bond coupling occurs through a CO dimer at the low overpotential, whereas the adsorbed COCHO on Cu(100) was identified as a key intermediate for producing C_2 products at high overpotentials, namely, CO reduction into adsorbed CHO species followed by reaction with adsorbed CO to form a COCHO intermediate, which is more favorable than CO dimerization.[26,27] Although extensive theoretical investigations on potential-dependent C−C coupling pathways on Cu(100), the exact C−C bond formation mechanisms toward C_2

products are still debated, and many aspects of the atomic-level details of this mechanism are still elusive due to the complexity of electrochemical interfaces.

The experimental observations and theoretical calculations have showed that CO is a key intermediate during CO_2 electroreduction on Cu electrodes since its further reduction can lead to similar product distribution as that of CO_2.[6,15,21,28−31] Furthermore, it was felt that CO further electroreduction is the rate-determining step of the reaction due to high implied CO coverage, by which CO_2 electroreduction kinetics can be determined on Cu electrode surfaces, thereby we can assume that pathway of CO_2 electrochemical reduction into CO on Cu electrodes is much faster than CO further electroreduction steps toward production of hydrocarbons, such as CH_4, C_2H_4, and alcohols, which may be able to lead to the abovementioned high implied CO coverage. Thus, we present a CO coverage-dependent electrochemical interface model on Cu(100) for the investigation of C−C coupling pathways taking place in production of C_2 products that enables us obtain potential-dependent C−C bond formation mechanisms in this paper. Our present employed methodology for the simulations is differentiated from the previous studies on C−C bond formation. Our recent established explicit solvation model involving two relaxed H_2O bilayer is employed to simulate the solvent effect,[32,33] which is of the essence in simulating electrochemical interfaces and allows us to better model the interactions among solvent, surface, and adsorbates. On the basis of this finding, this paper specifically focuses on the initial CO electroreduction and potential-dependent C−C bond formation pathways by applying a CO coverage-dependent interface model on the Cu surface, by which we can obtain a better mechanistic insight into the effect of Cu single-crystal surface on product selectivity and C−C coupling pathways toward C_2 products.

■ CO COVERAGE−DEPENDENT EQUILIBRIUM POTENTIALS

CO adsorption configurations and sites with various coverage can be observed on the Cu(100) surface, as can be seen in Figure S1. The adsorbed CO prefers to occupy 4-fold hollow sites when CO coverage (θ_{CO}) is below 1/9 monolayer (ML). Simultaneous adsorption of CO at 4-fold hollow and 2-fold bridge sites is found when θ_{CO} is in the range of 1/9 to 1/3 ML. We can observe the simultaneous occupation of 4-fold hollow, 2-fold bridge, and 1-fold top sites when θ_{CO} is 4/9 ML. Simultaneous adsorption of CO at 2-fold bridge and 1-fold top sites is found when θ_{CO} is in the range of 4/9 to 1 ML. CO molecules are found to only adsorb at 1-fold top site when θ_{CO} is 1 ML in order to minimize repulsive interactions. The conditions of θ_{CO} above 1 ML are not further considered in this paper because CO dimers can be formed spontaneously when θ_{CO} are above 1 ML (see Figure S1). As shown in Figure S2a, a reasonable polynomial relationship of adsorption isotherms between differential adsorption energy of CO [$\Delta E(\theta)$] and θ_{CO} is exhibited on Cu(100), suggesting that CO adsorption on Cu(100) may abide by Langmuir adsorption isotherms. $\Delta E(\theta)$ can be calculated by fitting of polynomial of the present $\Delta E(\theta) \sim \theta_{CO}$ data at any θ_{CO}. Thus, according to the eq S4, the polynomial dependence of the computational equilibrium potentials (U) on θ_{CO} can be obtained on Cu(100), as can be seen in Figure S2b. The equilibrium potential of *ca.* 0.40 V (*vs* RHE) can be obtained when θ_{CO} is equal to zero, being comparable with a required

value (*ca.* 0.17 V *vs* RHE) thermodynamically for CO_2 electroreduction on Cu electrodes and thereby considered as the required equilibrium potential thermodynamically in the present paper, validating reasonability of our used interface model to some extent. The increasing θ_{CO} will make equilibrium potential be more and more negative. Interestingly, we note that the present obtained adsorption isotherms on Cu(100) is differentiated from the linear relationship between $\Delta E(\theta)$ and θ_{CO} on Cu(111) that is proposed in our recent study,[33] in which the Termkin adsorption isotherms may be followed for adsorbed CO on Cu(111), suggesting that Cu single-crystal surface may be able to influence CO adsorption property. Thus, we can speculate that the difference of adsorption isotherms may be able to explain the effect of Cu single-crystal surface on product selectivity during CO_2 electroreduction, which is not involved in early theoretical and experimental studies. In this paper, the electroreduction pathways containing proton and electron transfer are simulated through direct transfer of adsorbed H atoms to surface adsorbed species at the present simulated electrode/solution interface.[34,35]

■ RESULTS AND DISCUSSION

Initial CO Reduction Pathways on Cu(111). The early experimental reports performed by Hori *et al.* showed that single-crystal surface of Cu exhibits high selectivity for C_1 and C_2 products during CO_2 electroreduction, namely, Cu(111) surface favors production of C_1 product like CH_4, and more open (100) facet of Cu exhibits excellent selectivity toward C_2 products.[9,36] On the basis of our recent proposed CO coverage-dependent Cu(111)/H_2O electrochemical interface model,[33] conditions of three electrode potentials are considered in order to obtain initial CO electroreduction pathways on Cu(111) and explain the effect of the crystal face on product selectivity at different applied potentials. The calculated equilibrium potential is *ca.* 0.10 V (*vs* RHE) when θ_{CO} is equal to 1/3 ML, corresponding to the condition of a low overpotential of *ca.* 0.17 V compared with the calculated thermodynamically required equilibrium potential of *ca.* 0.27 V when θ_{CO} is equal to zero on Cu(111). The equilibrium potential of *ca.* −0.15 V (*vs* RHE) is obtained when θ_{CO} is equal to 2/9 ML, which corresponds to the condition of a medium overpotential of *ca.* 0.42 V. When θ_{CO} is equal to 1/3 ML, the computational equilibrium potentials is *ca.* −0.50 V (*vs* RHE), corresponding to the conditions of high overpotentials of *ca.* 0.77 V. Three possible species involving the adsorbed CHO, COH, and dimer OCCO molecules may be able to be formed for initial CO reduction. As shown in Figure 1, at a low overpotential (θ_{CO} = 1/9 ML), the required activation barrier for the formation of CHO species is *ca.* 0.85 eV on Cu(111), being notably lower than that of COH formation (*ca.* 1.39 eV). Moreover, the formation pathway of COH species is strongly endothermic by 1.09 eV at the low overpotential, being significantly more positive than reaction free energy of the CHO formation pathway (*ca.* 0.65 eV). The barrier for the formation of the adsorbed dimer OCCO by CO dimerization is calculated as *ca.* 1.43 eV, being slightly higher than that of COH formation on Cu(111), and considerably more positive reaction free energy (*ca.* 1.38 eV) is also observed at the low overpotential, as shown in Figure 1. In the presence of a medium overpotential (θ_{CO} = 2/9 ML), the activation barrier and reaction free energy for CHO formation are almost unchanged, which are calculated as *ca.* 0.87 and 0.69
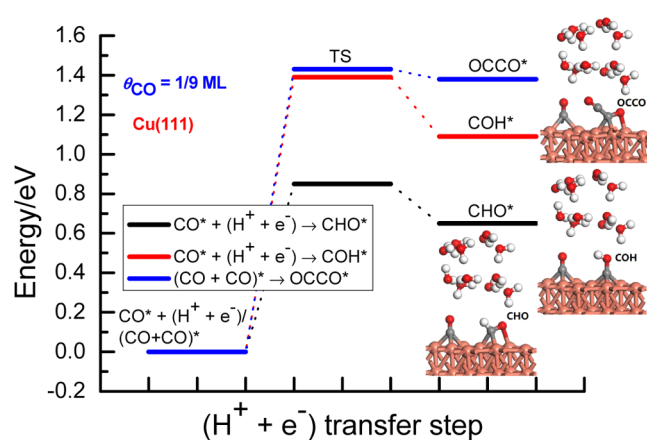

Figure 1. Energy pathway diagram of initial CO reduction to CHO, COH, and dimer OCCO intermediates on Cu(111) at a low overpotential (θ_{CO} = 1/9 ML) (* represents surface adsorption of species).

eV, respectively. However, formation of dimer OCCO has a relatively lower barrier than COH formation (*ca.* 1.30 *vs* 1.57 eV) at the medium overpotential, in which the formations of these both species are still strong endothermic processes (*ca.* 1.24 *vs* 1.10 eV), as shown in Figure 2. The almost identical
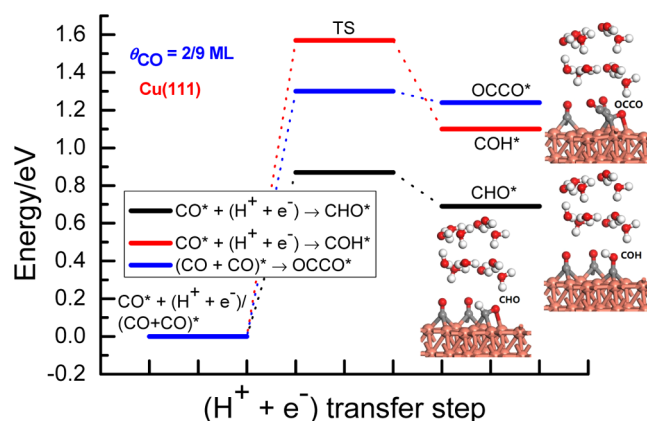

Figure 2. Energy pathway diagram of initial CO reduction to CHO, COH, and dimer OCCO intermediates on Cu(111) at a medium overpotential (θ_{CO} = 2/9 ML).

structure images of initial, transition, and final states may lead to almost unchanged barriers and reaction free energies for the initial CO electroreduction into CHO pathways at the low and medium overpotentials, as shown in Figures S3−S8, in which C−H and C−O bond lengths of the final state CHO are *ca.* 1.11 and 1.26 Å on Cu(111), respectively.

The presence of the higher overpotential (θ_{CO} = 1/3 ML) can significantly decrease the barriers and reaction energies for initial CO reduction into the adsorbed CHO, COH, and dimer OCCO species, as shown in Figure 3. The corresponding barrier is *ca.* 0.51, 1.29, and 0.96 eV, respectively, in which the required formation barrier for dimer OCCO is still lower than that of COH formation at the higher overpotential. The corresponding structure images of initial, transition, and final states can be seen in Figures S9−S11. Although the higher overpotential can make barriers of COH and OCCO formations decrease, they are still significantly higher than that of CHO formation. Thus, we can speculate that initial CO

reduction into the CHO intermediate is a more favorable pathway at various applied potentials based on energetics analysis. Simultaneously, we also note that the formed dimer OCCO by CO dimerization on Cu(111) is extremely unstable in conditions of three overpotentials, which is facile to back to adsorbed CO molecules with extremely low barriers of below 0.10 eV, as can be seen in Figures 2−4. In other words, the
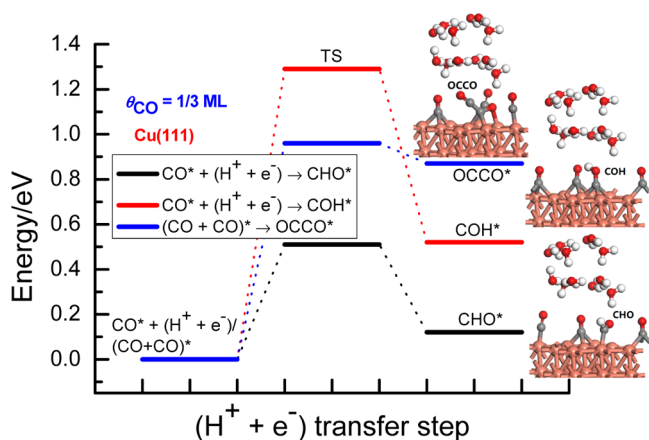

Figure 3. Energy pathway diagram of initial CO reduction to CHO, COH, and dimer OCCO intermediate on Cu(111) at a high overpotential (θ_{CO} = 1/3 ML).

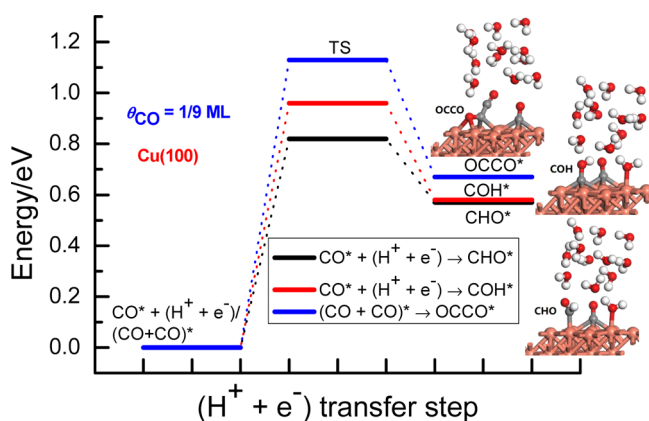**Figure 4.** Energy pathway diagram of initial CO reduction to CHO, COH, and dimer OCCO intermediate on Cu(100) at a low overpotential (θ_{CO} = 1/9 ML).

higher CO coverage on Cu(111) enables CHO formation to be more favorable. Thus, we can conclude that CHO is a key intermediate during initial CO reduction on Cu(111), which can finally lead to production of C_1 products, explaining experimentally the observed effect of the Cu single-crystal surface on product selectivity.

At the high overpotential, the significantly decreased barrier for CHO formation may be attributed to change in CHO adsorption configurations, in which the mixed C−O coordination configurations at the low and medium over-potentials are formed, whereas the coordination pattern of a single C atom is obtained at the high overpotential, as shown in Figures S3, S6, and S8. Our present conclusion for initial CO reduction into CHO species is well consistent with the recent experimental investigation conducted by Koper *et al.* for CO_2 reduction by using online electrochemical mass spectrometry,[7,22] in which the results indicated that CHO is

the possibly crucial intermediate for production of the CH_4 product on Cu(111).

C−C Bond Formation Mechanisms on Cu(100). The Cu(100) single-crystal electrode had been reported exper-imentally to have unique selectivity for C_2 products.[11] In this paper, three electrode potentials are considered to obtain potential-dependent C−C bond formation mechanisms on Cu(100). The calculated equilibrium potential is *ca.* 0.03 V (*vs* RHE) when θ_{CO} is 1/9 ML on Cu(100), which corresponds to the condition of a low overpotential of *ca.* 0.37 V compared with the present computational thermodynamically required equilibrium potentials when θ_{CO} is equal to zero. The equilibrium potential of *ca.* −0.08 V (*vs* RHE) can be obtained when θ_{CO} is equal to 2/9 ML, which corresponds to the condition of a medium overpotential of *ca.* 0.48 V. When θ_{CO} is equal to 1/3 ML, the calculated equilibrium potential is *ca.* −0.30 V (*vs* RHE), corresponding to the condition of a high overpotential of *ca.* 0.70 V. Thus, the initial CO reduction and C−C coupling pathways at different overpotentials can be calculated by employing the CO coverage-dependent electro-chemical interface model on Cu(100).

The initial CO reduction into adsorbed CHO, COH, and dimer OCCO intermediate is first considered to determine whether CO dimerization mechanism leads to C−C coupling on the pathway to the production of C_2 products on Cu(100). As can be seen in Figure 4, the barriers for the formations of CHO, COH, and dimer OCCO are calculated as *ca.* 0.82, 0.96, and 1.13 eV on Cu(100), respectively, indicating that the initial CO reduction prefers to form CHO species at the low overpotential, as observed on Cu(111). The increasing overpotentials change the initial CO reduction pathways, in which COH formation is the most favorable due to the lowest barrier of *ca.* 0.75 eV at the medium overpotential, as shown in Figure 5. The theoretical study from Asthagiri *et al.* also
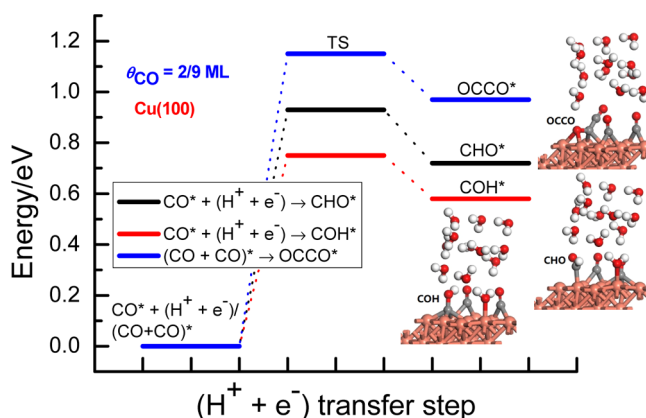

Figure 5. Energy pathway diagram of initial CO reduction to CHO, COH, and dimer OCCO intermediates on Cu(100) at a medium overpotential (θ_{CO} = 2/9 ML).

showed that the adsorbed COH species is more favorable than CHO on Cu(100) at relatively higher overpotentials,[23] confirming our present theoretical conclusion. However, CHO and COH species may be able to be simultaneously formed under the condition of high overpotential because of the almost equal and extremely low barriers of below 0.10 eV (see Figure 6). The corresponding structure images of initial, transition and final states on Cu(100) for adsorbed

intermediates CHO, COH, and dimer OCCO formations at various overpotentials are shown in Figures S12−S20.

At the various applied potentials, we find that the formation of dimer OCCO by CO dimerization on Cu(100) is always the most difficult to occur due to significantly higher barriers and more positive reaction free energies than those of CHO and COH formations. Furthermore, the increasing overpotentials can lead to increasing barriers of CO dimerization, as observed values of *ca.* 1.13, 1.15, and 1.37 eV (see Figures 5−7),
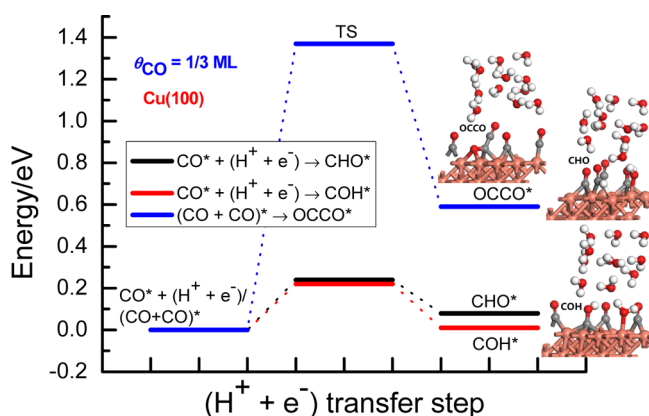

Figure 6. Energy pathway diagram of initial CO reduction to CHO, COH, and dimer OCCO intermediates on Cu(100) at a high overpotential (θ_{CO} = 1/3 ML).
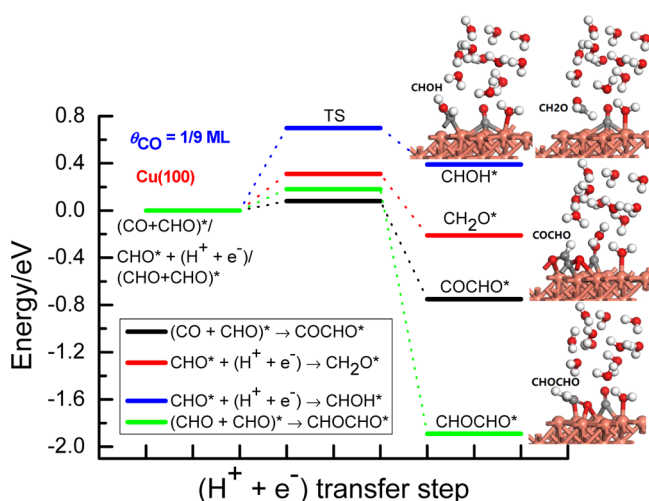

Figure 7. Energy pathway diagram of CHO further reduction into CH_2O, CHOH, and dimers COCHO and CHOCHO intermediates on Cu(100) at a low overpotential (θ_{CO} = 1/9 ML).

implying that the pathway of CO dimerization into C_2 species will close at various applied potentials. Thus, it can be speculated that dimer OCCO species may not be a reliable intermediate during CO_2 electroreduction to C_2 products on Cu(100). The present obtained conclusion exhibits excellent consistency with a previous theoretical study on the C−C bond formation mechanism from Head-Gordon *et al.*[26,27] Using time-resolved attenuated total reflection surface-enhanced infrared absorption spectroscopy, however, recent experimental study from Hwang *et al.* suggested that C−C bond formation exclusively takes place by CO dimerization into adsorbed OCCO intermediate toward C_2 products on prepared electrodeposited and sprayed power Cu electrodes,

without the participation of adsorbed CHO intermediate, which can lead to productions of C_1 products.[37] The inconsistencies of C−C coupling pathways may be able to be attributed to difference of employed crystal face of Cu surfaces, in which only fragmented Cu(100) single-crystal surface is used in our present theoretical work, whereas Cu electrodes with polycrystallinity may be prepared in the experimental investigation conducted by Hwang *et al.*

To explore alternative C−C bond formation mechanisms at various applied potentials on Cu(100), the further reduction processes of C_1 species formed by the initial CO reduction are carried out. Beginning with the most favorable CHO species at the low overpotential (θ_{CO} = 1/9 ML), four possibilities of CHO further reduction are considered, as shown in Figure 7. It is found that the required barriers for the formations of CH_2O and CHOH species are *ca.* 0.35 and 0.70 eV, respectively, being significantly higher than those of dimers COCHO and CHOCHO formations (*ca.* 0.10 and 0.18 eV, respectively). Moreover, the reaction of the adsorbed CHO with CO and the adsorbed CHO dimerization to dimers COCHO and CHOCHO species are strongly exothermic by −0.75 and −1.89 eV, respectively. Thus, we can conclude that the reaction pathway of CHO with CO and CHO dimerization exhibit C−C bond formation mechanisms at the low overpotential, and the formed dimers COCHO and CHOCHO will result in the production of C_2 products. The corresponding structure images of initial, transition, and final states at the low overpotential for CHO electroreduction into CH_2O, CHOH, and dimers COCHO and CHOCHO species on Cu(100) are exhibited in Figures S21−S24. Our present study on CHO dimerization into CHOCHO species is well consistent with the previous theoretical work performed by Asthagiri *et al.* using the linear kinetic barrier method on the basis of Butler−Volmer theory, in which C−C coupling occurs by two adsorbed CHO intermediates at low overpotentials, leading to the production of C_2 products like C_2H_4 on Cu(100).[23]

Under the condition of a medium overpotential (θ_{CO} = 2/9 ML), the energetics for COH further reduction is analyzed since initial CO reduction into COH is preferable. As shown in Figure 8, the activation barriers for formations of the adsorbed dimers COCOH and COHCOH species through the reaction of COH with CO and COH dimerization both are calculated as *ca.* 0.10 eV and surmountable at room temperature with a negative reaction free energy of *ca.* −0.72 and −1.76 eV, respectively, being notably lower than those of C along with H_2O and CHOH formations on Cu(100). Therefore, we can speculate that C−C bond coupling occurs preferentially through the reaction of adsorbed COH with CO species and COH dimerization at the medium overpotential, and the formation of dimers COCOH and COHCOH will lead to the production of C_2 products. The corresponding structure images of initial, transition, and final states for COH electroreduction into various possible species on Cu(100) at the medium overpotential can be seen in Figures S25−S28. In fact, the most recent experimental study from Pérez-Gallent *et al.* had shown that a hydrogenated dimer COCOH species is detected using Fourier transformation infrared spectroscopy at the potentials of *ca.* −0.10 V (*vs* RHE) in CO electroreduction on Cu(100),[19] confirming reasonability of our present used theoretical model and accuracy of conclusions.

At the present simulated high overpotential (θ_{CO} = 1/3 ML), simultaneous formations of CHO and COH species can

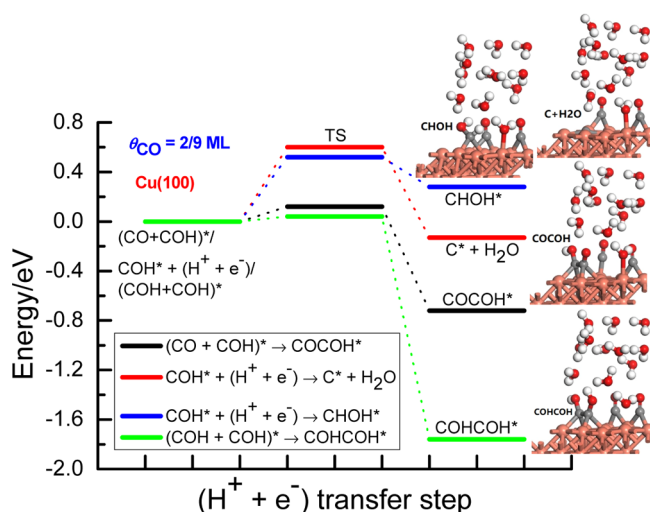**Figure 8.** Energy pathway diagram of COH further reduction into C along with H_2O, CHOH, and dimers COCOH and COHCOH species on Cu(100) at a medium overpotential (θ_{CO} = 2/9 ML).

be concluded on Cu(100) based on the above energetics. Thus, CHO and COH further reduction processes and interactions of the adsorbed CHO with COH species are considered. As can be seen in Figure 9, it is found that the
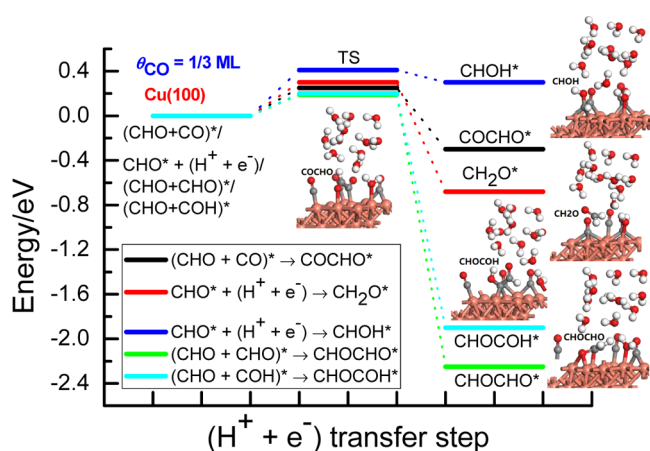

Figure 9. Energy pathway diagram of CHO further reduction into CH_2O, CHOH, dimers COCHO, CHOCHO, and CHOCOH species on Cu(100) at a high overpotential (θ_{CO} = 1/3 ML).

activation barrier for reactions of the adsorbed CHO with CO, COH, and CHO to form dimers COCHO, CHOCOH, and CHOCHO is *ca.* 0.25, 0.20, and 0.19 eV, respectively, being all lower than those of CH_2O and CHOH formations. With the barriers of the adsorbed COH further reduction into C along with H_2O formation, dimers COCOH and COHCOH are significantly increased to *ca.* 1.75, 0.80, and 0.56 eV at the high overpotential, respectively, whereas the CHOH formation barrier is almost unchanged (*ca.* 0.50 eV) in contrast with that at medium overpotential, as shown in Figure 10. The corresponding structure images of initial, transition, and final states for CHO and COH electroreduction are shown in Figures S29−S37. By comparing the adsorption configurations of initial states for dimers COCOH and COHCOH formation pathways at the medium and high overpotentials, it is observed that the distance between C atoms in the adsorbed CO and COH species increases from *ca.* 2.77 to 2.84 Å as the
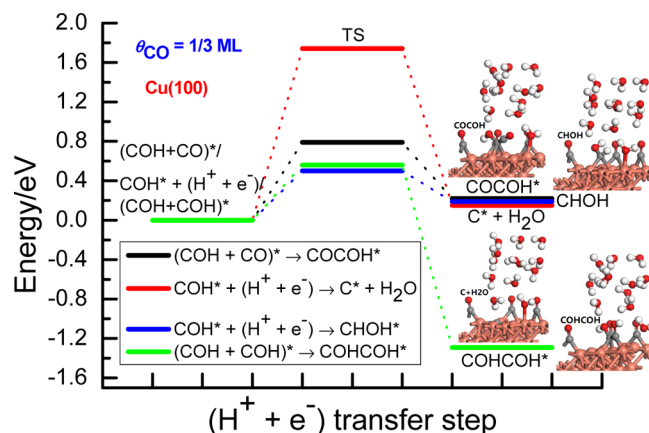

Figure 10. Energy pathway diagram of COH further reduction into CHOH, C along with H_2O formation, dimers COCOH and COHCOH species on Cu(100) at a high overpotential (θ_{CO} = 1/3 ML).

overpotentials increase, and the corresponding distance between the adsorbed COH species also increases from *ca.* 3.02 to 3.07 Å. Thus, we can conclude that the repulsive interactions between the co-adsorbed CO and COH species and between the co-adsorbed COH species on Cu(100) at the high overpotential may lead to difficult formations of dimers COCOH and COHCOH.

By comparing the barriers of CHO and COH further reduction, we find dimers COCHO, CHOCOH, and CHOCHO formations *via* the reactions of CHO with CO, COH, and CHO require significantly lower barriers than those of COH further reduction and can be overcome at room temperature on Cu(100) at the high overpotential. Therefore, it can be concluded that the formed dimers COCHO, CHOCOH, and CHOCHO may lead to production of C_2 products at the high overpotential, which are regarded as the C−C coupling pathway. Formed COH species may be only able to react with CHO species during CO_2 electroreduction on Cu(100) due to significant higher barriers for its further reduction into C along with H_2O formation, dimers COCOH and COHCOH, which can result in CHOCOH formation. In earlier theoretical reports from Head-Gordon *et al.* on C−C bond formation mechanisms on Cu(100),[26,27] COCHO species was also identified as an important intermediate toward production of C_2 products at high overpotentials, validating our present conclusion to some degree. The optimal C−C bond formation mechanisms on Cu(100) can be presented at the simulated electrode/solution interface by scrutinizing the above energy pathway diagram at various applied potentials, as shown in Figure 11.

Our present conclusions for C−C bond coupling mechanisms on Cu(100) are partially inconsistent with recent experimental observations. For instance, the experimental study by using *in situ* electrochemical attenuated total reflection Fourier transform infrared spectroscopy combined with density functional theory (DFT) calculations from Wang *et al.* showed that C−C coupling occurs by only adsorbed intermediate CHO dimerization during productions of C_2 products on fluorine-modified Cu catalysts.[38] The crystalline structure and the morphology of electrodes may determine the difference of C−C coupling pathways, in which the high-resolution transmission electron microscopy results showed that Cu(111) facet could be formed, and it is also selected as a
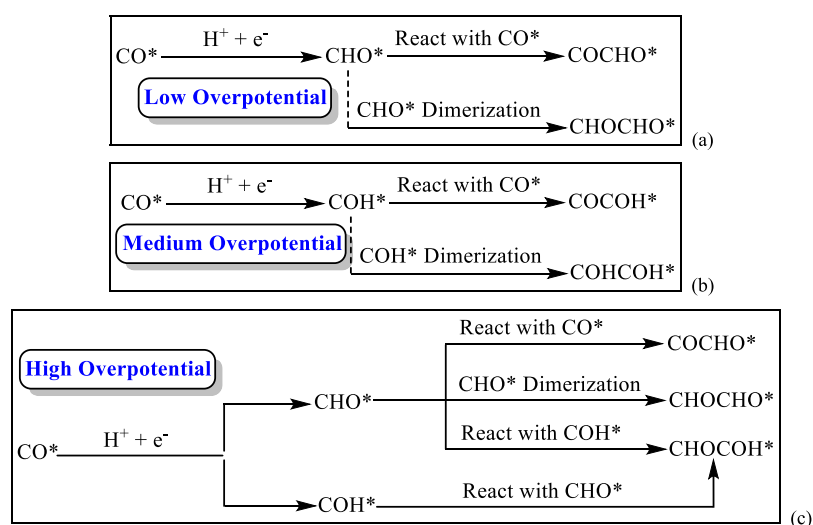
Figure 11. Optimal C−C bond formation mechanism at the present simulated electrode/solution interface on Cu(100): (a) at the low overpotential; (b) at the medium overpotential; and (c) at the high overpotential.

crystal face for CO_2 reduction to C_2 products in DFT calculations from Wang et al. The C−C coupling intermediate COCOH was identified experimentally by Fourier transform infrared spectroscopy studies combined with DFT calculations during photocatalytic CO_2 reduction on CuO(111) surface conducted by Sheng et al.[39] Similarly, the difference of the selected crystal face may result in partially different C−C coupling pathways. Additionally, the experimental studies on formation mechanisms of the C−C coupled intermediate have been possibly limited in that the spectroscopically detected species must be relatively stable during CO_2 electroreduction, which may also be able to lead to difference of C−C coupling mechanisms between our present theoretical calculations and recent experimental observations. In fact, cation effects, such as alkaline-metal adatoms Li, Na, K, and Cs, have a significant effect on the CO_2 electrochemical reduction reaction rate and mechanism, in which electrostatic interactions play an important role in the alkaline-metal promotion effect. However, the cation effect is not involved in our present employed electrode/solution interface model, leading to no comparison between our calculated results and some existing experimental and theoretical data, which will be further considered in our next work.

CONCLUSIONS

In this paper, we present a CO coverage-dependent electro-chemical interface model on Cu(100) with explicit solvent effect for studying C−C coupling pathways occurring during production of C_2 products that enables us obtain theoretical insights into potential-dependent C−C bond formation mechanisms. Our results show that CHO is a crucial intermediate on Cu(111) toward the production of C_1 products, and dimer OCCO may not be a reliable intermediate toward C_2 products on Cu(100). At the low overpotential, the reaction pathway of CHO with CO and CHO dimerization exhibit C−C bond formation mechanisms, and the formed dimers COCHO and CHOCHO may result in production of C_2 products. However, C−C coupling takes place preferentially through the reaction of COH with CO species and COH dimerization, and dimers COCOH and COHCOH formations on Cu(100) may result in production of C_2 products at the

medium overpotential. The formed dimers COCHO, CHOC-OH, and CHOCHO through the reactions of CHO with CO, COH, and CHO species may lead to the production of C_2 products, which are regarded as C−C bond formation mechanisms at the high overpotential. The formed COH species may be only able to react with CHO species on Cu(100), which can result in CHOCOH formation. The difference of obtained adsorption isotherms of CO on Cu(100) and Cu(111) may be able to explain the effect of Cu single-crystal surface on product selectivity during CO_2 electroreduction. Our present conclusions exhibit excellent consistency with the available experimental reports and partial theoretical studies, confirming the reasonability of our present used electrode/solution interface model.

MODEL AND COMPUTATIONAL DETAILS

Surface and solvation models, computational parameters, and determination methodologies for CO coverage-dependent equilibrium potentials on Cu(100) have been elaborated in the Supporting Information. Our present employed method-ology for the simulations is different from the early theoretical studies on CO_2 electroreduction mechanisms. For example, Calle-Vallejo et al. suggested that dimer OCCO on Cu(100) via an Eley−Rideal mechanism can preferably be formed based on the computational hydrogen electrode model,[12] which is the relevant precursor to the production of C_2 species. However, this model to stabilize CO dimer lacks rigorous treatment of electrode/solution interfaces and cannot calculate potential-dependent kinetic barriers. Asthagiri et al. reported facet dependence of CO_2 electroreduction pathways on Cu electrodes using the linear kinetic barrier method based on Butler−Volmer theory with only one or two relaxed H_2O molecules,[23] in which CHO formation is preferred on Cu(100), and C_2H_4 can be produced via C−C coupling of two adsorbed CHO intermediates at relatively lower over-potentials. The previous used computational hydrogen electrode model and linear kinetic barrier method only considered the effect of the external electric field on electrocatalytic reaction mechanisms and neglected the effect of the internal electric field on the adsorption configuration of reaction species. In fact, the effect of the internal electric field

should not be neglected in order to more accurately model electrocatalytic reaction mechanisms. In this manuscript, the electrode potential can be adjusted by changing CO coverage (θ_{CO}), and the increasing θ_{CO} will result in increasing negative equilibrium potential, in which internal electric field may be changed by changing θ_{CO}, thereby theoretical insights into the potential-dependent C−C bond formation pathways occurring during CO_2 electroreduction into C_2 products can be obtained by calculating reaction free energies and kinetic barriers.

ASSOCIATED CONTENT

Ⓢ Supporting Information

The Supporting Information is available free of charge at https://pubs.acs.org/doi/10.1021/acsomega.1c01062.

> Surface and solvation models, computational parameters, CO coverage-dependent electrode/solution interface models, various possible surface CO adsorption configurations on Cu(100) at different CO coverage, polynomial relationships between CO coverage and the differential adsorption energy of CO, polynomial dependence of the calculated equilibrium potentials on CO coverage on Cu(100), and geometry for C−C bond formation pathways under the conditions of three overpotentials (PDF)

AUTHOR INFORMATION

Corresponding Authors

Lihui Ou − Hunan Province Cooperative Innovation Center for the Construction & Development of Dongting Lake Ecologic Economic Zone, Hunan Provincial Key Laboratory of Water Treatment Functional Materials, Hunan Province Engineering Research Center of Electroplating Wastewater Reuse Technology, College of Chemistry and Materials Engineering, Hunan University of Arts and Science, Changde 415000, China; orcid.org/0000-0001-5177-2404; Email: lihuiou@huas.edu.cn

Hai Yang − Hunan Provincial Key Laboratory of Environmental Catalysis & Waste Recycling, Hunan Institute of Engineering, Xiangtan 411104, PR China; Email: yanghai1001@163.com

Authors

Zixi He − Hunan Province Cooperative Innovation Center for the Construction & Development of Dongting Lake Ecologic Economic Zone, Hunan Provincial Key Laboratory of Water Treatment Functional Materials, Hunan Province Engineering Research Center of Electroplating Wastewater Reuse Technology, College of Chemistry and Materials Engineering, Hunan University of Arts and Science, Changde 415000, China

Yuandao Chen − Hunan Province Cooperative Innovation Center for the Construction & Development of Dongting Lake Ecologic Economic Zone, Hunan Provincial Key Laboratory of Water Treatment Functional Materials, Hunan Province Engineering Research Center of Electroplating Wastewater Reuse Technology, College of Chemistry and Materials Engineering, Hunan University of Arts and Science, Changde 415000, China

Complete contact information is available at:
https://pubs.acs.org/10.1021/acsomega.1c01062

Notes

REFERENCES

(1) Costentin, C.; Robert, M.; Savéant, J.-M. Catalysis of the Electrochemical Reduction of Carbon Dioxide. *Chem. Soc. Rev.* **2013**, *42*, 2423−2436.

(2) Wang, W.; Wang, S.; Ma, X.; Gong, J. Recent Advances in Catalytic Hydrogenation of Carbon Dioxide. *Chem. Soc. Rev.* **2011**, *40*, 3703−3727.

(3) Gattrell, M.; Gupta, N.; Co, A. Electrochemical Reduction of CO_2 to Hydrocarbons to Store Renewable Electrical Energy and Upgrade Biogas. *Energy Convers. Manage.* **2007**, *48*, 1255−1265.

(4) Verma, S.; Kim, B.; Jhong, H.-R. M.; Ma, S.; Kenis, P. J. A. A Gross-Margin Model for Defining Technoeconomic Benchmarks in the Electroreduction of CO_2. *ChemSusChem* **2016**, *9*, 1972−1979.

(5) Jouny, M.; Luc, W.; Jiao, F. General Techno-Economic Analysis of CO_2 Electrolysis Systems. *Ind. Eng. Chem. Res.* **2018**, *57*, 2165−2177.

(6) Kuhl, K. P.; Cave, E. R.; Abram, D. N.; Jaramillo, T. F. New Insights into the Electrochemical Reduction of Carbon Dioxide on Metallic Copper Surfaces. *Energy Environ. Sci.* **2012**, *5*, 7050−7059.

(7) Schouten, K. J. P.; Qin, Z.; Pérez Gallent, E.; Koper, M. T. M. Two Pathways for the Formation of Ethylene in CO Reduction on Single-Crystal Copper Electrodes. *J. Am. Chem. Soc.* **2012**, *134*, 9864−9867.

(8) Hori, Y.; Wakebe, H.; Tsukamoto, T.; Koga, O. Electrocatalytic Process of CO Selectivity in Electrochemical Reduction of CO_2 at Metal Electrodes in Aqueous Media. *Electrochim. Acta* **1994**, *39*, 1833−1839.

(9) Hori, Y.; Takahashi, I.; Koga, O.; Hoshi, N. Electrochemical Reduction of Carbon Dioxide at Various Serials of Copper Single Crystal Electrodes. *J. Mol. Catal. A: Chem.* **2003**, *199*, 39−47.

(10) Xie, M. S.; Xia, B. Y.; Li, Y.; Yan, Y.; Yang, Y.; Sun, Q.; Chan, S. H.; Fisher, A.; Wang, X. Amino Acid Modified Copper Electrodes for the Enhanced Selective Electroreduction of Carbon Dioxide towards Hydrocarbons. *Energy Environ. Sci.* **2016**, *9*, 1687−1695.

(11) Hori, Y.; Takahashi, I.; Koga, O.; Hoshi, N. Selective Formation of C_2 Compounds from Electrochemical Reduction of CO_2 at a Series of Copper Single Crystal Electrodes. *J. Phys. Chem. B* **2002**, *106*, 15−17.

(12) Calle-Vallejo, F.; Koper, M. T. M. Theoretical Considerations on the Electroreduction of CO to C_2 Species on Cu(100) Electrodes. *Angew. Chem., Int. Ed.* **2013**, *52*, 7282−7285.

(13) Montoya, J. H.; Peterson, A. A.; Nørskov, J. K. Insights into C-C Coupling in CO_2 Electroreduction on Copper Electrodes. *ChemCatChem* **2013**, *5*, 737−742.

(14) Montoya, J. H.; Shi, C.; Chan, K.; Nørskov, J. K. Theoretical Insights into a CO Dimerization Mechanism in CO_2 Electro-reduction. *J. Phys. Chem. Lett.* **2015**, *6*, 2032−2037.

(15) Kortlever, R.; Shen, J.; Schouten, K. J. P.; Calle-Vallejo, F.; Koper, M. T. M. Catalysts and Reaction Pathways for the Electrochemical Reduction of Carbon Dioxide. *J. Phys. Chem. Lett.* **2015**, *6*, 4073−4082.

(16) Ou, L.; Long, W.; Chen, Y.; Jin, J. New Reduction Mechanism of CO Dimer by Hydrogenation to C_2H_4 on a Cu(100) Surface:

Theoretical Insight into the Kinetics of the Elementary Steps. *RSC Adv.* **2015**, *5*, 96281−96289.

(17) Figueiredo, M. C.; Ledezma-Yanez, I.; Koper, M. T. M. In situ spectroscopic Study of CO_2 Electroreduction at Copper Electrodes in Acetonitrile. *ACS Catal.* **2016**, *6*, 2382−2392.

(18) Wuttig, A.; Liu, C.; Peng, Q.; Yaguchi, M.; Hendon, C. H.; Motobayashi, K.; Ye, S.; Osawa, M.; Surendranath, Y. Tracking a Common Surface-Bound Intermediate during CO_2-to-Fuels Catalysis. *ACS Cent. Sci.* **2016**, *2*, 522−528.

(19) Pérez-Gallent, E.; Figueiredo, M. C.; Calle-Vallejo, F.; Koper, M. T. M. Spectroscopic Observation of a Hydrogenated CO Dimer Intermediate during CO Reduction on Cu(100) Electrodes. *Angew. Chem., Int. Ed.* **2017**, *56*, 3621−3624.

(20) Gunathunge, C. M.; Li, X.; Li, J.; Hicks, R. P.; Ovalle, V. J.; Waegele, M. M. Spectroscopic Observation of Reversible Surface Reconstruction of Copper Electrodes under CO_2 Reduction. *J. Phys. Chem. C* **2017**, *121*, 12337−12344.

(21) Gattrell, M.; Gupta, N.; Co, A. A Review of the Aqueous Electrochemical Reduction of CO_2 to Hydrocarbons at Copper. *J. Electroanal. Chem.* **2006**, *594*, 1−19.

(22) Schouten, K. J. P.; Kwon, Y.; van der Ham, C. J. M.; Qin, Z.; Koper, M. T. M. A New Mechanism for the Selectivity to C_1 and C_2 Species in the Electrochemical Reduction of Carbon Dioxide on Copper Electrodes. *Chem. Sci.* **2011**, *2*, 1902−1909.

(23) Luo, W.; Nie, X.; Janik, M. J.; Asthagiri, A. Facet Dependence of CO_2 Reduction Paths on Cu Electrodes. *ACS Catal.* **2016**, *6*, 219−229.

(24) Montoya, J. H.; Shi, C.; Chan, K.; Nørskov, J. K. Theoretical Insights into a CO Dimerization Mechanism in CO_2 Electroreduction. *J. Phys. Chem. Lett.* **2015**, *6*, 2032−2037.

(25) Sandberg, R. B.; Montoya, J. H.; Chan, K.; Nørskov, J. K. CO-CO Coupling on Cu Facets: Coverage, Strain and Field Effects. *Surf. Sci.* **2016**, *654*, 56−62.

(26) Goodpaster, J. D.; Bell, A. T.; Head-Gordon, M. Identification of Possible Pathways for C−C Bond Formation during Electrochemical Reduction of CO2: New Theoretical Insights from an Improved Electrochemical Model. *J. Phys. Chem. Lett.* **2016**, *7*, 1471−1477.

(27) Garza, A. J.; Bell, A. T.; Head-Gordon, M. Mechanism of CO_2 Reduction at Copper Surfaces: Pathways to C_2 Products. *ACS Catal.* **2018**, *8*, 1490−1499.

(28) Dewulf, D. W.; Jin, T.; Bard, A. J. Electrochemical and Surface Studies of Carbon Dioxide Reduction to Methane and Ethylene at Copper Electrodes in Aqueous Solutions. *J. Electrochem. Soc.* **1989**, *136*, 1686−1691.

(29) Kim, J. J.; Summers, D. P.; Frese, K. W., Jr. Reduction of CO_2 and CO to Methane on Cu Foil Electrodes. *J. Electroanal. Chem.* **1988**, *245*, 223−244.

(30) Hori, Y.; Murata, A.; Takahashi, R.; Suzuki, S. Electroreduction of Carbon Monoxide to Methane and Ethylene at a Copper Electrode in Aqueous Solutions at Ambient Temperature and Pressure. *J. Am. Chem. Soc.* **1987**, *109*, 5022−5023.

(31) Peterson, A. A.; Abild-Pedersen, F.; Studt, F.; Rossmeisl, J.; Nørskov, J. K. How Copper Catalyzes the Electroduction of Carbon Dioxide into Hydrocarbon Fuels. *Energy Environ. Sci.* **2010**, *3*, 1311−1315.

(32) Ou, L. Theoretical Insights into the Effect of Solvation and Sublayer Ru on Pt-Catalytic CH_3OH Oxidation Mechanisms in the Aqueous Phase. *J. Phys. Chem. C* **2018**, *122*, 14554−14565.

(33) Ou, L.; Chen, J.; Chen, Y.; Jin, J. Mechanistic Study on Cu-Catalyzed CO_2 Electroreduction into CH_4 at Simulated Low Overpotentials Based on an Improved Electrochemical model. *Phys. Chem. Chem. Phys* **2019**, *21*, 15531−15540.

(34) Cheng, T.; Xiao, H.; Goddard, W. A., III Reaction Mechanisms for the Electrochemical Reduction of CO_2 to CO and Formate on the Cu(100) Surface at 298 K from Quantum Mechanics Free Energy Calculations with Explicit Water. *J. Am. Chem. Soc.* **2016**, *138*, 13802−13805.

(35) Cheng, T.; Xiao, H.; Goddard, W. A., III Free-Energy Barriers and Reaction Mechanisms for the Electrochemical Reduction of CO on the Cu(100) Surface, Including Multiple Layers of Explicit Solvent at pH 0. *J. Phys. Chem. Lett.* **2015**, *6*, 4767−4773.

(36) Hori, Y.; Murata, A.; Takahashi, R. Formation of Hydrocarbons in the Electrochemical Reduction of Carbon Dioxide at a Copper Electrode in Aqueous Solution. *J. Chem. Soc., Faraday Trans.* **1989**, *85*, 2309−2326.

(37) Kim, Y.; Park, S.; Shin, S.-J.; Choi, W.; Min, B. K.; Kim, H.; Kim, W.; Hwang, Y. J. Time-Resolved Observation of C-C Coupling Intermediates on Cu Electrodes for Selective Electrochemical CO_2 Reduction. *Energy Environ. Sci.* **2020**, *13*, 4301−4311.

(38) Ma, W.; Xie, S.; Liu, T.; Fan, Q.; Ye, J.; Sun, F.; Jiang, Z.; Zhang, Q.; Cheng, J.; Wang, Y. Electrocatalytic Reduction of CO_2 to Ethylene and Ethanol through Hydrogen-Assisted C-C Coupling over Fluorine-Modified Copper. *Nat. Catal.* **2020**, *3*, 478−487.

(39) Wang, W.; Deng, C.; Xie, S.; Li, Y.; Zhang, W.; Sheng, H.; Chen, C.; Zhao, J. Photocatalytic C-C Coupling from Carbon Dioxide Reduction on Copper Oxide with Mixed-Valence Copper(I)/Copper(II). *J. Am. Chem. Soc.* **2021**, *143*, 2984−2993.